energies

MDPI

Article

Synergistic Germanium-Decorated h-BN/MoS_2 Heterostructure Nanosheets: An Advanced Electrocatalyst for Energy Storage Applications

M. Saravanan [1,2,†], Rajkumar Palanisamy [3,†], V. Sethuraman [4,*], K. Diwakar [1,5], P. Senthil Kumar [1], P. Sundara Venkatesh [6], N. Kannan [6], R. Joel Kingston [1], K. Aravinth [1] and Jinho Kim [3,*]

1 Research Centre, Sri Sivasubramaniya Nadar College of Engineering, Kalavakkam, Chennai 603110, Tamil Nadu, India
2 Department of Physics, University College of Engineering, Bharathidasan Institute of Technology Campus, Anna University, Tiruchirapalli 620024, Tamil Nadu, India
3 Department of Mechanical Engineering, Yeungnam University, Gyeongbuk-do, Gyeongsan-si 38541, Republic of Korea
4 Research and Development, New Energy Storage Technology, Lithium-ion Battery Division, Amara Raja Battery Ltd., Karakambadi, Tirupati 517520, Andhra Pradesh, India
5 Mechanical Engineering and Applied Mechanics, University of Pennsylvania, 3205 Walnut Street, Philadelphia, PA 19104, USA
6 Nanomaterials Laboratory, Department of Physics, Sri S. Ramasamy Naidu Memorial College, Sattur 626203, Tamil Nadu, India
* Correspondence: sethur182@gmail.com (V.S.); jinho@ynu.ac.kr (J.K.)
† These authors contributed equally to this work.

Abstract: Increasing concerns about the vulnerability of the world's energy supply and the necessity to implement sustainable technologies have prompted researchers to develop high-performance electrocatalysts that are affordable and efficient for converting and storing renewable energy. This article reports a facile approach to fabricating two-dimensional (2D) Ge-decorated h-BN/MoS_2 heterostructure nanosheets by self-assembly for multiple electrochemical applications such as supercapacitor and hydrogen evolution reactions. The organization of the physical and chemical links between the germanium modulations on the heterostructure of boron nitride/molybdenum sulphide (Ge/h-BN/MoS_2) were facilitated to generate more active sites. Furthermore, the asymmetric supercapacitor of Ge-decorated h-BN/MoS_2 amplified the capacitance to 558.53 F g^{-1} at 1 A g^{-1} current density and 159.19 F g^{-1} at 10 A g^{-1}, in addition to a retention rate of 85.69% after 2000 cycles. Moreover, the Ge-decorated h-BN/MoS_2 catalyst realized a low over-potential value, with an RHE of 0.57 (HER) at 5 mA/cm^2, a Tafel value of ∼204 mV/dec, and long-term electrolysis stability of 10 h. This work may open the door for further investigations on metal-decorated heterostructures, which have a significant potential for both supercapacitor and water-splitting applications.

Keywords: electrocatalysis; hydrogen evolution reaction; Ge/h-BN/MoS_2; energy storage application; layered heterostructure

check for updates

Citation: Saravanan, M.; Palanisamy, R.; Sethuraman, V.; Diwakar, K.; Kumar, P.S.; Venkatesh, P.S.; Kannan, N.; Kingston, R.J.; Aravinth, K.; Kim, J. Synergistic Germanium-Decorated h-BN/MoS_2 Heterostructure Nanosheets: An Advanced Electrocatalyst for Energy Storage Applications. *Energies* **2023**, *16*, 3286. https://doi.org/10.3390/en16073286

Academic Editor: Nicu Bizon

Received: 3 March 2023
Revised: 31 March 2023
Accepted: 1 April 2023
Published: 6 April 2023

1. Introduction

Due to the quick depletion of non-renewable energy resources, high energy demand and environmental pollution have been addressed by focusing on stimulating interest in sustainable and renewable energy. The alarm about environmental pollution and high energy demand means that green energy and high-performance, eco-friendly energy production/storage systems are immediately required in energy technology engineering [1–3]. Electrocatalytic approaches are one of the most appealing and efficient storage technologies for producing high-pure fuels, high energy density, and sustainable energy sources to meet the demands of energy consumption. Therefore, the development of effective and

reliable electrocatalysts is mandatory to speed the electrocatalytic (especially HER and OER) processes to create highly pure oxygen/hydrogen effectively [4]. On the cathode side of the electrodes, a 2e− transfer assists the hydrogen evolution reaction (HER), and on the anode side, a 4e− transfer assists the oxygen evolution reaction (OER). Both sides have a pair of half-cell reactions throughout the water splitting process.

Commercial noble metal Pt hybrids/alloys for HER and Ir/Ru oxides/alloys for OER electrocatalysts currently exhibit benchmark electrocatalytic properties (long-term stability and low overpotentials) and are widely regarded as exceptional electrocatalysts [5]. Recently, several bimetallic nanohybrids based on Mo and Ni sulphide and other materials, such as Ni-MoS2 [6], NiS/MoS_2 [7], and MoS2/NiS_2 [8], have demonstrated significant promise as cost-effective electrode materials for water splitting due to their prudently tuned synergistic effects and favourable interface architecture. He et al. [9] created hydrothermal graphene/metallic MoS_2 nanostructure heterostructures for a hydrogen assessment catalyst, while MoS_2/WS_2 heterostructures were constructed by Kim et al. [10] for increased hydrogen assessment methods. As a result, a great deal of work has gone into developing efficient electrocatalysts composed of materials that are devoid of noble metals [11]. However, most of them are concerned only with HER or OER electrocatalytic activity. Developing efficient electrocatalysts that enhance both HER and OER for total water splitting has remained a major issue thus far. The development of earth-abundant materials that allow effective conversion efficiency and storage is a critical problem for realizing such green energy systems. However, as far as we know, there is not enough research on Ge/h-BN/MoS_2 nanohybrids for energy conversion and storage.

Owing to their distinct physical and chemical characteristics, metal decorations containing heterostructures have sparked widespread interest as a class of appealing earth-abundant materials for supercapacitor applications. Research communities are increasingly considering non-noble-metal-based electrocatalysts such as transition-metal chalcogenides, transition-metal oxides, hydroxides, carbides, nitrides, and phosphates, which are less expensive and highly efficient [12–14]. The naturally abundant MoS_2, composed of trigonal prismatic Mo and S molecular lamellae, possesses semiconducting properties that make it a highly efficient and cost-effective material for electrolysis. By increasing the thickness of the molybdenum sulphide from a single sheet, it may be possible to enhance the bandgap from 1.3 eV to 1.9 eV [15].

Catalytic support, lubrication, self-clean coatings, electronic devices, and other applications of h-BN, commonly known as white graphene, have all been proven. Unlike graphene, h-BN has a wide bandgap (6.0 eV), which makes it unsuitable for photocatalytic applications. Chemical functionalization and doping of heteroatoms can change the electrical structure of h-BN. Hybrid materials and nanocomposites based on h-BN have recently been shown to be attractive prospects for electrochemical applications [16]. However, to achieve the same level of tunability in three dimensions as traditional semiconductors (e.g., Ge, Si, etc.), additional research into interface control and a material assay of homogenous 2D materials is required. The decoration of 2D materials and 3D semiconductors with and without dangling bonds on the surface has been investigated from the standpoint of the perfect preparation of three-dimensional materials by weak Van der Waals contact. Meanwhile, boron nitride, a 2D material with a high bandgap and a smooth surface, has been successfully used to create several Van der Waals heterostructures, such as graphene/h-BN, MoS_2/h-BN, phosphorene/h-BN, and Bi/Sb (111) [17]. Binary composites have also been reported in several places. Furthermore, it has been shown that binary rGO composites have outstanding electrochemical characteristics. Jiao et al. [18] found that a MoS_2/rGO composite produced using the hydrothermal method shows good electrochemical characteristics with about 95% of capacitance retention. At a current density of 0.2 A g^{-1}, E. Iyyamperumal et al. [19]. found that vertically oriented BCN nanotubes have a 321 F g^{-1} specific capacitance. Because MoS_2 and Ge can store lithium ions, the overall electrode energy density is improved up to three times over graphite, with 1700 mAh/cm^3 by volumetric capacity [20]. MoS_2/rGO demonstrate exceptional electrochemical characteristics,

with more than 1200 F g^{-1} specific capacitance, according to the report of Zhao et al. [21]. A MoS_2/graphene layer-controlled aerogel composite at a 100 mA g^{-1} current density, with a specific capacitance of much more than 1000 mA g^{-1}, was also reported to have a reversible capacity [22]. The goal of our current research is to develop a simple chemical approach to evaluate the electrochemical characteristics of a Ge/h-BN/MoS_2 heterostructure. The structure of the h-BN/MoS_2 material effectively addresses the concern regarding the enormous volume variation that occurs throughout the germanium process. In another way, the rational hybridization of h-BN/MoS_2 and Ge is mutually advantageous in addressing their respective inherent electrochemical flaws. The multi-element synergized h-BN/MoS_2 nanosheets provide excellent supercapacitor and electrocatalytic performance in addition to long-term electrolysis stability. In a two-electrode-cell configuration, Ge/h-BN/MoS_2 was employed for the study for uses like supercapacitors and water splitting.

2. Materials and Methods

All the compounds employed in this study were AR-grade components that were not purified further, such as oleylamine (OLA, $C_{18}H_{37}N$, 70%) and germanium (−100 mesh, ≥99.9). Hexagonal boron nitride (h-BN) micro powder and molybdenum sulphide (MoS_2) (98% purity) were purchased from SRL products. N-methyl pyrrolidone (NMP, C_5H_9NO, Merck) was used without additional distillation.

2.1. Synthesis of h-BN/MoS_2 Heterostructures

To prepare the h-BN/NMP dispersion, 10 mg of h-BN was dispersed in 100 mL of NMP solvent using sonication for 1 h. After that, 20 mg of bulk MoS_2 was added to the h-BN/NMP solutions and thoroughly mixed. The resulting solutions were ultrasonically combined for 30 min, agitated for 24 h at room temperature, and centrifuged at 4000 rpm for 30 min. The top liquid was eliminated, and the solid precipitation, h-BN/MoS_2 heterostructures, was obtained.

2.2. Synthesis of Ge-Decorated h-BN/MoS_2 Heterostructures

Toluene and oleylamine (15 mL) were added after Ge and h-BN/MoS_2 were mixed in a 2:1 weight ratio (30 mL). After vigorously agitating the solution for 12 h at room temperature, the Ge/h-BN/MoS_2 composites were produced by centrifuging 5 mL toluene and 35 mL ethanol three times at 8000 rpm for 10 min. Furthermore, heat of 350 °C for 2 h was used to remove excess oleylamine ligands on the surface of the Ge nanoparticles in an atmosphere-free furnace, which can overcome the poor electrical conductivity. After annealing, the Ge/h-BN/MoS_2 nanohybrids were taken out and used in the tests to determine exactly what their structures and performance were (Figure 1).

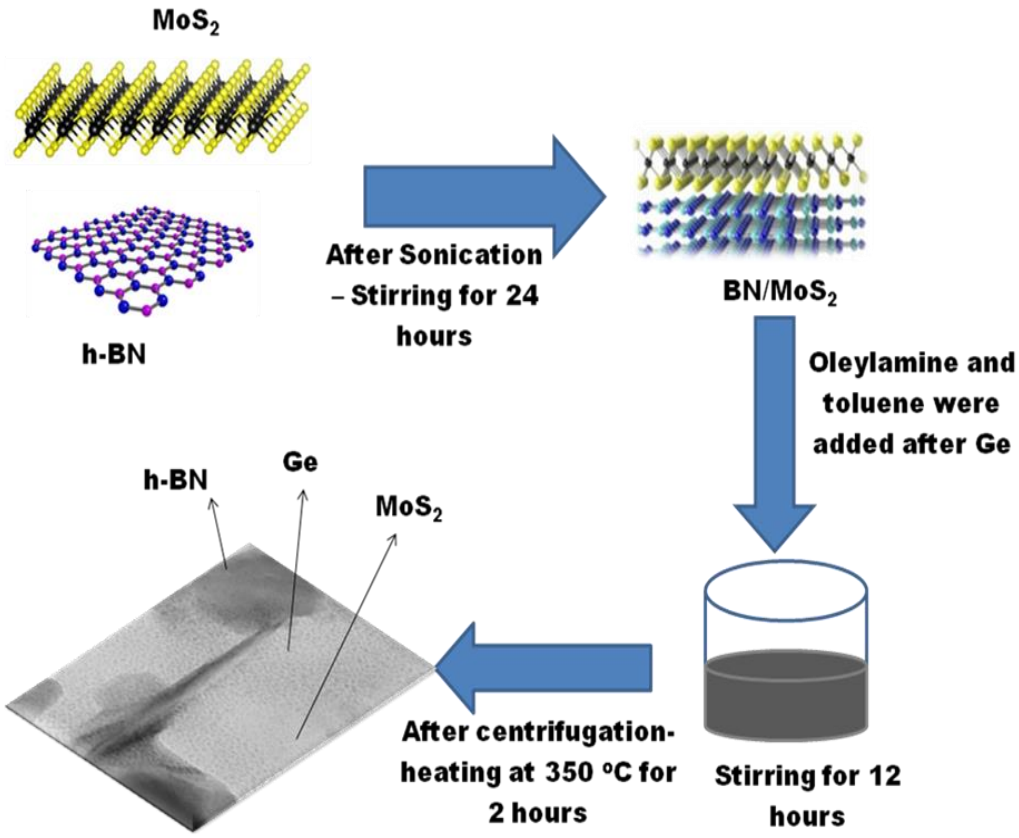

Figure 1. Formation mechanisms of Ge-modulated h-BN/MoS_2.

3. Characterization

The phase of the Ge/BN/MoS_2 catalyst was identified using X-ray diffraction (XRD, Cu kα using X-Pert pro-PANalytic) with λ = 1.54178 Å. The surface functional groups and bonding nature of h-BN/MoS_2 and Ge/h-BN/MoS_2 were determined using FTIR (JASCO 460 PLUS, Pfungstadt, Germany) in the range of 400 to 4000 cm^{-1}. Transmission electron microscopy (TEM, JEOL, Akishima, Tokyo, Japan) with a 200 kV accelerating voltage was used to characterize the surface morphology and physiochemical structure of Ge/h-BN/MoS_2. The configuration details on the surface of the synthesized Ge/BN/MoS_2 material were examined using an ESCALab250 X-ray photoelectron spectrometer (XPS). The allowed sample size depends on the instrument configuration, but commonly, samples on the order of $\sim 1 \times 1$ cm^2 and less than 1 cm high can be analysed in most systems.

All the electrocatalysis studies for OER/HER using Ge/h-BN/MoS_2 electrocatalysts were displayed on an electrochemical measurement performed (CH Instruments Inc., Bee Cave, TX, USA) using the standard. All electrochemical measurements were carried out using a standard three-electrode electrochemical workstation (K-Lyte 1.3 potentiostat) with MoS_2 coated glassy carbon (GC), platinum rod, and Ag/AgCl electrode used as the working electrode, the counter electrode, and the reference electrode, respectively. According to the equation below, all potentials were rectified versus reversible hydrogen electrodes (RHE). In 0.5 M H_2SO_4, ERHE = ESCE + 1.01 V. Typically, 0.004 g of 1 mL of mixed (700 µL of water and 300 µL of ethanol) as-sonicated catalyst was added, and then 100 µL Nafion (10 wt%) was added. After 20 min of ultrasonication, an ink solution was obtained. Desiccated ink catalysts were dropped onto a glassy carbon electrode (GCE, catalyst loading 0.4 mg cm^2) and dried in a 50 °C oven. Linear sweep voltammetry (LSV) and double-layer capacitances (Cdl) were performed at various sweep rates and frequency ranges of 105 to 0.1 Hz, while electrochemical impedance spectroscopy (EIS) was also performed. Chronoamperometric I versus t curve tests were also performed to find out how stable the Ge/h-BN/MoS_2/GCE system was after it was fixed.

Electrode Preparation for Energy Storage Applications

The prepared electrodes were analysed for supercapacitor application in order to determine the best material. For the preparation of the working electrode, carbon black, PVDF, and the active material were combined in a ratio of 10:10:80. These components were ground using a mortar and pestle, and NMP was added drop-wise to form a homogenous slurry. The slurry was coated with 11 cm of Ni foam and dried for 12 h at 90 °C in a hot-air oven. The dried electrode was used in a conventional three-electrode system consisting of a working electrode (active material), Pt (counter), and Ag/AgCl (reference) with 2 M of potassium hydroxide (KOH) as an electrolyte. The CHI60 electrochemical workstation was used to investigate the cyclic voltammetry (CV) and galvanostatic charge/discharge (GCD) of the electrode. The capacitance from the CV graph was calculated using the formula given below [23]:

$$C_{sp} = \frac{\int IdV}{2mv\Delta V} \tag{1}$$

Here, current is I, the scan rate is v, the active material mass is m, and the potential window is V. The following equation was used to compute the specific capacitance of the electrode materials from a GCD plot.

$$C_{sp} = \frac{I\Delta t}{\Delta V \times m} \tag{2}$$

Here, I denotes current, t denotes discharge duration, V denotes potential window, and m denotes material mass (g).

4. Results and Discussion

4.1. Physicochemical Characterizations of Ge/h-BN/MoS$_2$

The crystalline features of h-BN/MoS$_2$ and Ge-modulated h-BN/MoS$_2$ were evaluated with XRD analysis. Figure 2a shows the XRD pattern of taken h-BN power that exhibits diffraction peaks at 26.6°, 41.8°, and 43.90°, which correspond to the (002), (100), and (101) [JCPDS: 34-0421] planes that are indexed. The MoS$_2$ shows crystalline peaks at 14.2°, 32.5°, 33.5°, 35.8°, 39.5°, 49.0°, 58.40°, and 60.1°, corresponding to the (002), (100), (101), (102), (103), (105), (110), and (008) planes, and suggests the layered hexagonal structure of MoS$_2$ according to the file number 03-065-1951. Two types of diffraction peaks can be seen in the XRD pattern of the h-BN/MoS$_2$ hybrid. The extra peaks are closely matched with the lattice structures of the MoS$_2$ sheets in addition to the typical diffraction properties of the h-BN sheets. The preparation of Ge/h-BN/MoS$_2$ leads to the diffraction peaks that emerged at 27.2°, 45.3°, 53.7°, 65.8°, and 72.8° being indexed as (111), (220), (311), (400), and (331). This clearly shows that the Ge nanocomposites form themselves with h-BN and MoS$_2$. FTIR was also employed to characterise the chemical structure of h-BN/MoS$_2$ and Ge/h-BN/MoS$_2$ and to determine the surface functional groups and bonding nature, as shown in Figure 2b.

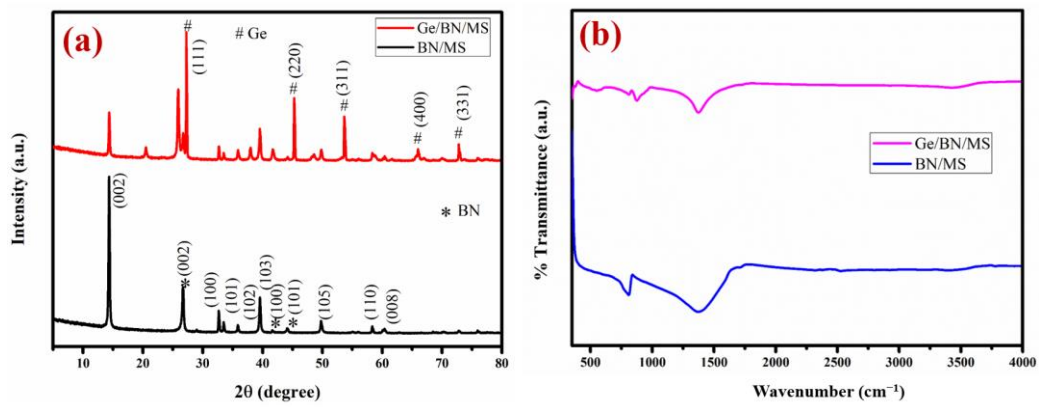

Figure 2. (**a**) XRD, (**b**) IR spectra of h-BN/MoS$_2$ and Ge-modulated h-BN/MoS$_2$.

The two peaks at 1369 cm^{-1} and 870 cm^{-1} for h-BN/MoS_2 are allocated to the boron-nitrogen-boron (B-N-B) bending mode and the boron-nitrogen (B-N) in-plane stretching mode, respectively, while the hydroxyl groups that are adsorbed on the MoS_2 nanosheets are assigned to 3439 cm^{-1} and 1692 cm^{-1}. The bending mode is attributed to the positively charged hydroxyl present on the MoS_2 [24,25]. The creation of a Ge-N bond is evident in the absorption bands at 791 cm^{-1}, clearly confirming the interaction between h-BN/MoS_2 and Ge. From the above FTIR results, it can be said that Ge-, h-BN-, and MoS_2-based nanocomposites have been achieved.

XPS survey spectral analysis was carried out to confirm the presence of boron (B), nitrogen (N), molybdenum (Mo), sulphur (S), and germanium (Ge) elements in the obtained Ge/h-BN/MoS_2, as shown in Figure 3.

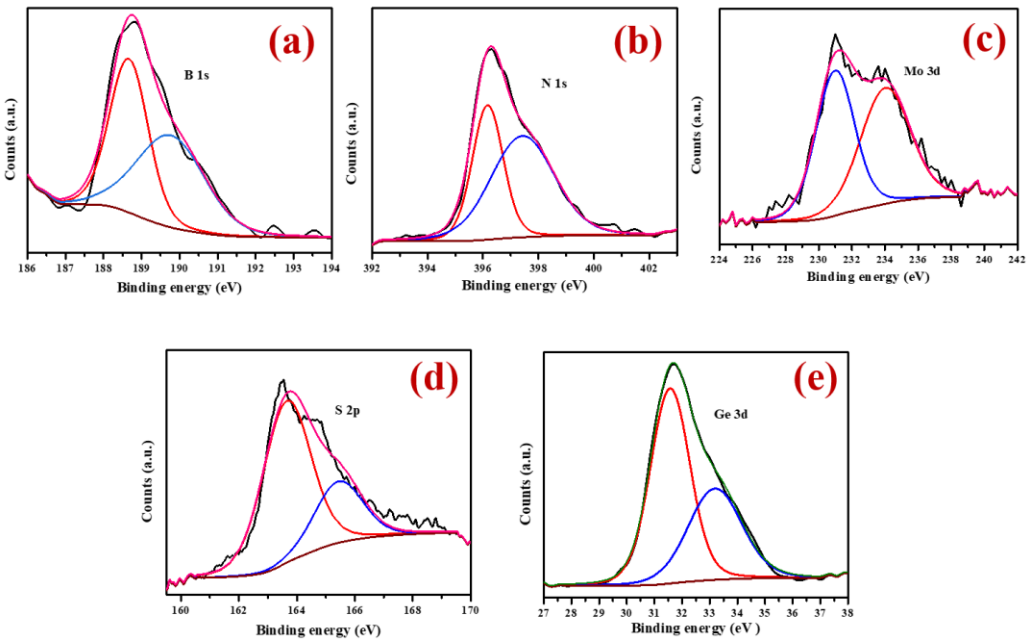

Figure 3. High-resolution (**a**) B 1s, (**b**) N 1s, (**c**) Mo 3d, (**d**) S 2p, and (**e**) Ge 3d XPS spectra of Ge/h-BN/MoS_2. The presence of Ge 3d, Mo 3d, and S 2p features suggest the growth of Ge nanoparticles embedded into the h-BN/MoS_2 network.

To understand the bonding pattern, high-resolution spectra of each individual element were examined. XPS spectra of the boron core-level emission (B 1s) and nitrogen core-level emission (N 1s) (Figure 3a,b) revealed the network of B-N bonding in h-BN, which were centred at binding energies (BEs) of 188.89 and 397.2 eV, respectively. The molybdenum (Mo 3d) core-level emission spectra corresponding to h-BN/MoS_2 result in well-resolved peaks at BEs of 230.9 and 234.4 eV, indicating spin-orbit components Mo 3d3/2 and Mo 3d3/2, respectively, in Figure 3c [26]. The S 2p spectra (Figure 3d) of MoS_2 nanosheets in the S^{2-} oxidation state exhibit a peak at 162.4 eV and broaden toward higher BEs. Because each MoS_2 sheet has a low grafting density and a restricted number of lamellae, the S 2p spectra produced a weak signal that could not be resolved in S 2p2/3 and 2p1/2 orbits-based peaks [27,28]. Ge 3d exhibits a large peak below 31.8 eV in its XPS spectra (Figure 3e), which can be attributed to Ge.

The direct development of Ge on nanosized MoS_2 sheets over platelets of h-BN is confirmed by the XPS spectra of the distinctive components.

HRTEM was used to explore the nanostructure characteristics and surface morphology of h-BN/MoS_2 and Ge/h-BN/MoS_2 hybrid materials. The MoS_2 nanosheets were consistently formed across the h-BN nanosheets in the h-BN/MoS_2 materials, as shown in Figure 4a,b (surface morphology), Figure 4c (lattice pattern), and Figure 4d (SAED pattern). Each MoS_2 nanosheet is made up of molecular lamellae, with greater resolution imaging

and lattice fringes in the inset. This shows that the sheets have crystallized significantly. The 2D structure grew with an average particle size of 50–55 nm.

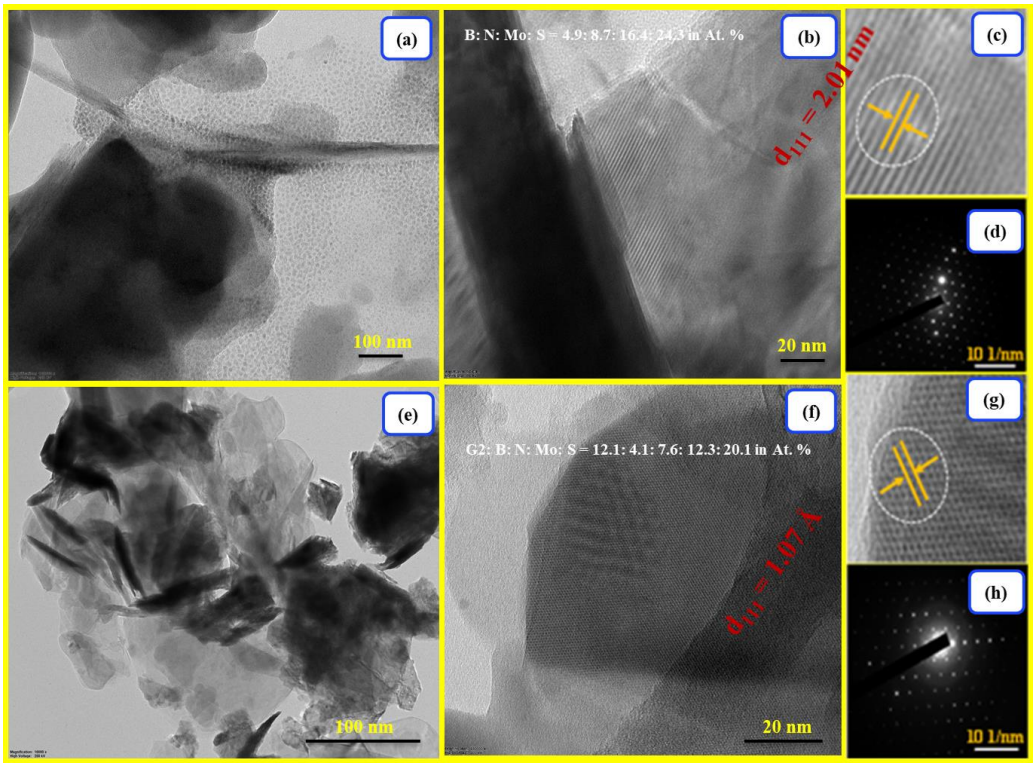

Figure 4. HRTEM images of (**a**–**d**) h-BN/MoS_2 and (**e**–**h**) Ge/h-BN/MoS_2.

Similarly, the germanium-incorporated MoS_2 nanosheets were also formed across the h-BN nanosheets in the Ge/h-BN/MoS_2 hybrid materials, as shown in Figure 4e,f (surface morphology), Figure 4g (lattice pattern), and Figure 4h (SAED pattern). MoS_2 initially formed a small 2D nucleus and then expanded into a large 2D crystal on h-BN while accumulating germanium crystals, according to the Frank–Van der Merwe mechanism. The h-BN/MoS_2 and Ge/h-BN/MoS_2 nanocomposites also have diffraction rings and a bright spot in their SAED patterns. This shows that the nanocomposites are polycrystalline.

4.2. Supercapacitor Performances

The energy storage capability of the prepared electrodes was analysed by subjecting them to CV and GCD techniques. Figure 5 shows the CV curve obtained for h-BN, MoS_2, h-BN/MoS_2, and Ge/h-BN/MoS_2 at scan rates in the range of 10 and 100 mV s^{-1} within a −0.2 to 0.6 V potential window. Pseudocapacitive behaviour is evident from the CV graphs, as they depict oxidation and reduction peaks. The active material stability was determined with the diffusion of KOH into the active material. At a lower scan rate, the KOH electrolyte can move around more easily. This means that the supercapacitor has a higher capacitance at a lower scan rate than at a higher rate.

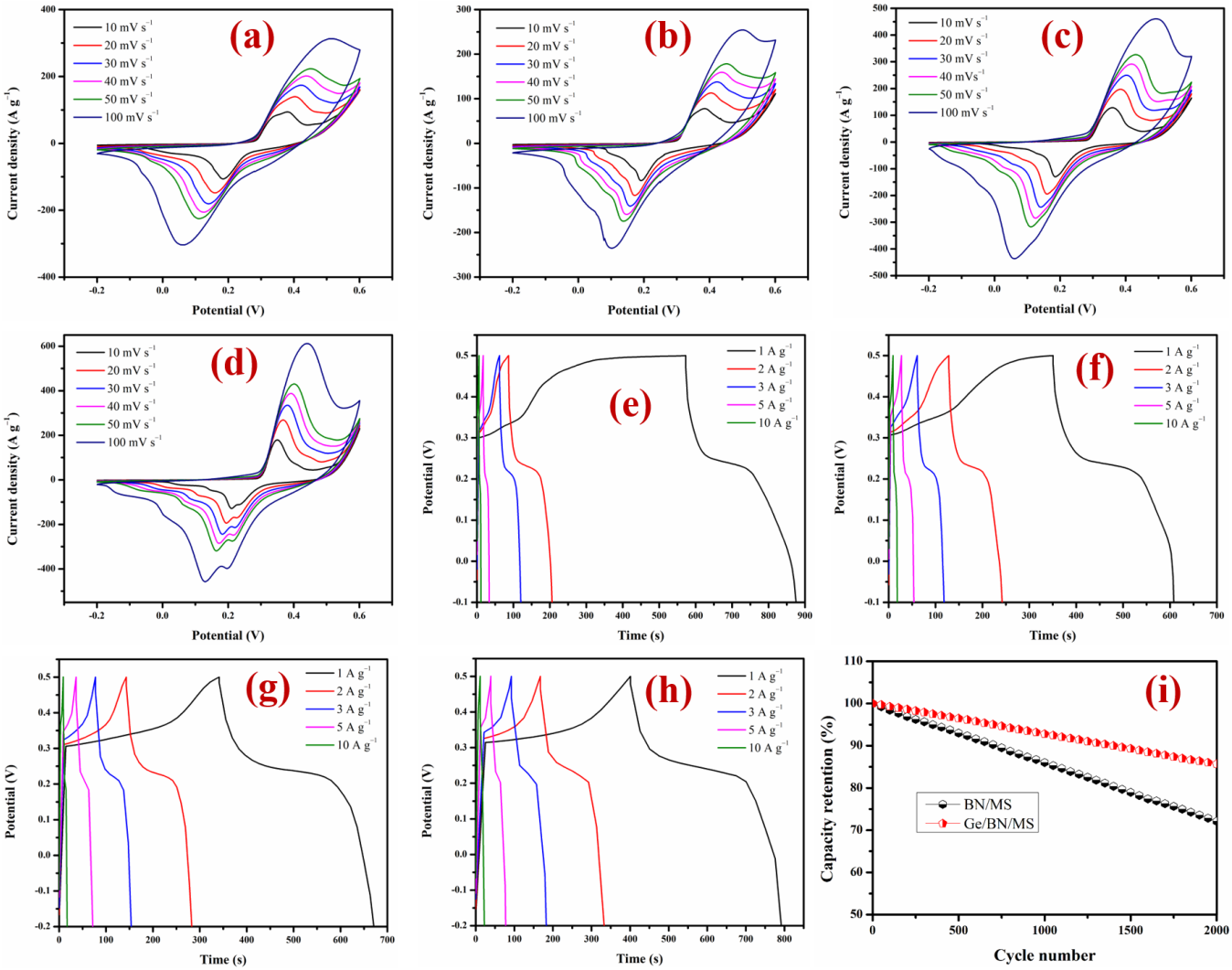

Figure 5. (**a**,**e**) CV and GCD of h-BN, (**b**,**f**) CV and GCD of MoS_2, (**c**,**g**) CV and GCD of h-BN/MoS_2, (**d**,**h**) CV and GCD of Ge/h-BN/MoS_2, and (**i**) capacity retention of h-BN/MoS_2 and of Ge/h-BN/MoS_2 nanohybrid.

It is evident that the capacitance of h-BN ranges from 765.44 F g^{-1} to 317.68 F g^{-1} for scan rates in the range of 10 and 100 mV s^{-1}, whereas MoS_2 delivers a capacitance of 572.06 F g^{-1} at 10 mV s^{-1}, which is lower than h-BN. The composite h-BN and MoS_2 (i.e., h-BN/MoS_2) delivered capacitance as high as 814.85 F g^{-1}. It is evident from Figure 5c that the h-BN/MoS_2 shows excellent reversibility of the h-BN/MoS_2 electrode, as there is no apparent deviation in the characteristic CV loops. From the CV plots of h-BN (Figure 5a), MoS_2 (Figure 5b), and h-BN/MoS_2 (Figure 5c), the area encircled by the loop appears to improve on incorporating MoS_2 into h-BN. The capacitance of h-BN/MoS_2 decreases in the order 814.85, 733.84, 680.13, 639.07, 600.38, and 478.38 F g^{-1} for scan rates in the series of 10, 20, 40, 60, 80, and 100 mV s^{-1}. The supercapacitor system is seen to deliver a remarkable specific capacitance of up to 927.78 F g^{-1} at a 10 mV s^{-1} scan rate, due to the introduction of Ge onto the h-BN/MoS_2 composite (Figure 5d). Even at a lower scan rate, 10 mV s^{-1}, the capacitance delivered is satisfactory, at 546.26 F g^{-1}. Herein, with an increase in the scan rate, capacitance increases as follows: 927.78, 821.84, 753.69, 698.37, 651.78, and 546.26 F g^{-1}.

The distorted triangular peaks in the charge/discharge profiles of h-BN and MoS_2 within the potential window of 0.4 V indicate the electrode shows pseudocapacitance. The formation of an h-BN/MoS_2 composite enhanced the capacitance. The h-BN/MoS_2

GCD curve (Figure 5g) shows that the capacitance increases significantly from 431.9 F g^{-1} to 470.956 F g^{-1} due to the addition of MoS_2. The alignment of MoS_2 sheets among the h-BN sheets improves the surface area and augments the accessibility of electrolytes into the active site, thereby delivering better performance. The addition of Ge to the h-BN/MoS_2 composite increases capacitance to 558.53 F g^{-1} at 1 A g^{-1} current density and to 159.19 F g^{-1} at 10 A g^{-1} current density, as shown in Figure 5h. The synergic effect of favourable defective sites along with the conductive Ge matrix not only exhibits OER electrocatalytic distinction, but also delivers exceptional capacitance. The consistency in the shape of the GCD curves of the active materials under study reveals the stability of the electrode material after a continuous charge–discharge cycle. Stability is an important factor for real-life applications of supercapacitor electrodes. Both h-BN/MoS_2 and Ge/h-BN/MoS_2 underwent 2000 charge/discharge cycles (Figure 5i). Ge/h-BN/MoS_2 kept 85.69% of its original capacity, while h-BN/MoS_2 kept 72.09%. Ge/h-BN/MoS_2 is more stable because it is a good electrical conductor, has a larger surface area, and has a low charge transfer resistance. When compared with several of the reported materials and their manufacturing, as shown in Table 1, the Ge/h-BN/MoS_2 material can be an efficient electrode material and demonstrates superior electrochemical behaviour for supercapacitor applications [29–37].

Table 1. Comparison of specific capacitance and capacitance retention.

S. No	Samples	Cs (Fg^{-1})	Retention	Cycle Number	References
1	Boron and nitrogen co-doped porous carbon	504 (1 Ag^{-1})	91	10,000	[29]
2	MoS_2 nanodots	122 (1 Ag^{-1})	86	1000	[30]
3	MoS_2/rGO@PANI	160 (1 Ag^{-1})	-	-	[31]
4	MoS_2 nanostructures/PEDOT	244 (1 Ag^{-1})	92	9000	[32]
5	Boron/nitrogen co-doped carbon	330 (0.5 Ag^{-1})	89	5000	[33]
6	MoS_2-rGO/PEDOTNP	298 (1 Ag^{-1})	93	10,000	[2]
7	PANI/Nitrogen-doped carbon composites	276 (0.2 Ag^{-1})	80	5000	[34]
8	H-NrGO/PANI	510 (1 Ag^{-1})	74	2000	[35]
9	rGO/PANI nanofiber	442 (0.3 Ag^{-1})	84	2000	[36]
10	Polyaniline/boron-doped graphene nanohybrid	406 (0.5 Ag^{-1})	83	5000	[37]
11	BCN/ MoS_2-11	283 (1 Ag^{-1})	-	-	[1]
12	Ge/BN/MoS_2	558 (1 Ag^{-1})	85	2000	This work

4.3. Electrocatalytic Examinations of Ge/h-BN/MoS_2/GCE

The electrocatalytic excellence of Ge/h-BN/MoS_2 modified on GCE was assessed using a standard three-electrode system containing alkaline 0.5 M H_2SO_4. the OER performances of h-BN and MoS_2 samples were also compared in the control, as shown in Figure 6a. The h-BN, MoS_2, h-BN/MoS_2, and Ge/h-BN/MoS_2 exhibited the overall potential of (η_{10}) 0.54, 0.56, 0.62, and 0.67. An anodic peak of oxidation at around a potential of 1.7 V (versus RHE) was observed on Ge/h-BN/MoS_2; this could be attributable to the amorphous metal hydroxide layer intermediate stage of development. Two primary features in the LSV polarization data for Ge/h-BN/MoS_2 and h-BN/MoS_2 nanostructures were obtained, which reveal a rise in the polarization signals associated with the germanium/molybdenum ion oxidation located after 1.7 V, as shown in Figure 6a. Moreover, the oxidation current starts to rise quickly after the potential value of 1.7 V versus RHE along with the little bubble appearance on the surface of the Ge/h-BN/MoS_2 modified carbon electrode, which reflects the proceeding of oxygen evolution. By measuring the LSV polarization potential values with respect to the theoretical oxygen evolution potential, the overpotential (η_{10}) of Ge/h-BN/MoS_2 was calculated with a reliable overpotential of 0.67 mV at 5 mA/cm^2.The measured overpotential values of Ge/h-BN/MoS_2 were

identified to be higher than the germanium-free h-BN/MoS_2 nanohybrid, i.e., 0.62 mV. Strikingly, this overpotential decrease in the presence of germanium could be ascribed to the effect of synergistic between the revealed active sites, with a lot of defects supported by Ge conductive support (Ge/h-BN/MoS_2 nanohybrid). Furthermore, the obtained OER results highlight that the Ge/h-BN/MoS_2 nanohybrid shows remarkable oxygen bubble desorption performance. Overall, the findings support Ge/h-BN/MoS_2 kinetics and electrocatalytic activity for OER. Furthermore, the OER stability (Figure 6c) and HER stability (Figure 6f) of the chronoamperometry tests were used to examine the Ge/h-BN/MoS_2 electrode during a 10 h period. In the OER study, there is no noticeable change in the initial current densities and potential in these tests, indicating consistent conductivity, mass transport, and durability. The h-BN, MoS_2, h-BN/MoS_2, and Ge/h-BN/MoS_2 exhibit a current density of 5.5, 7.8, 12.8, and 17.1 mA/cm^2, respectively. Similarly, the EIS data (Figure 6b) obtained in the Nyquist graphs display much fewer semicircles corresponding to Ge/h-BN/MoS_2 compared with h-BN/MoS_2, indicating lower resistance. The Ge/h-BN/MoS_2 catalyst's greater conductivity is attributable to the Ge conductive framework, making it easier for electrical charges to move and reducing the chance of Ohmic losses [38].

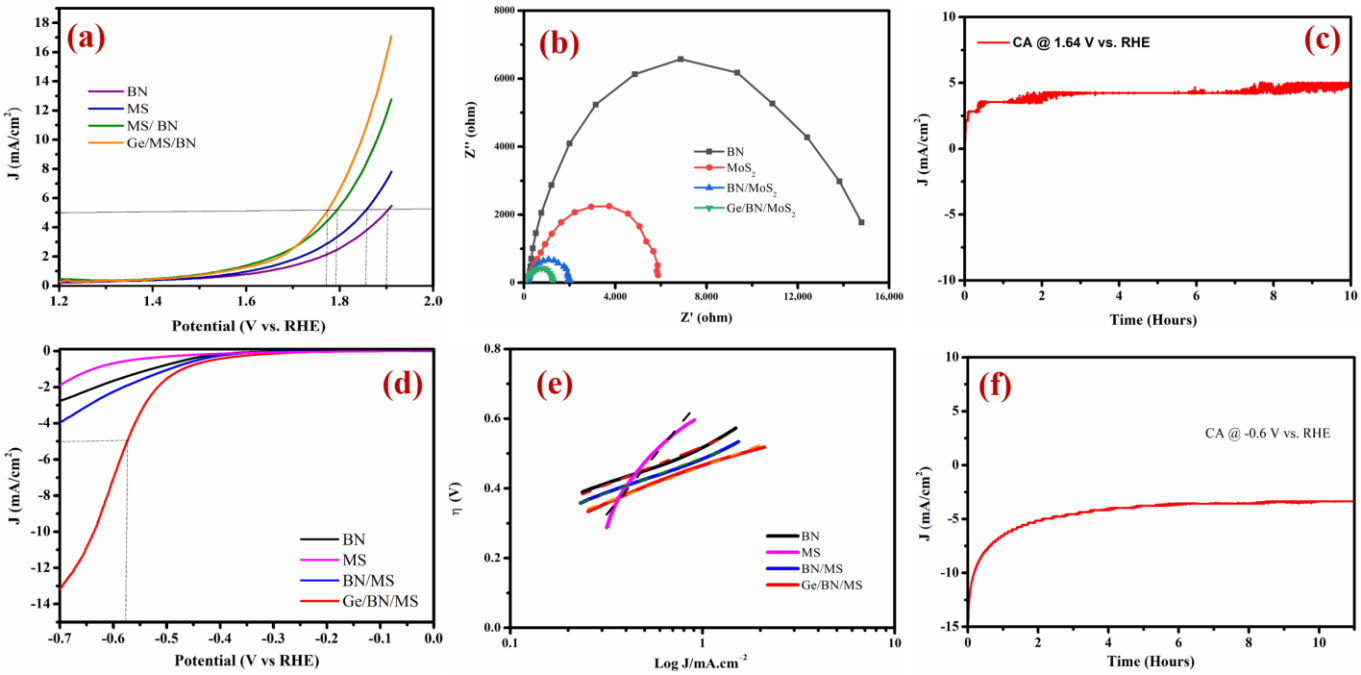

Figure 6. Electrocatalytic performance (**a**) OER, (**b**) EIS, (**c**) CA of h-BN/MoS_2, (**d**) HER, (**e**) Tafel, and (**f**) CA of Ge/h-BN/MoS_2 nanohybrid. The dotted lines are fitted curve of the tafel slope.

The HER electrocatalytic performance of the Ge/BN/MoS_2 nanohybrid was examined using LSV curves at a scan rate of 5 mVs^{-1} between 0.5 and 0.1 V versus RHE in an Ar-saturated aqueous 0.5 M H_2SO_4 solution, respectively. For comparison, pure h-BN and MoS_2 nanosheets, as well as Ge/h-BN/MoS_2 nanohybrids, were tested for HER performance. For a blank control, pure boron nitride sheets with no catalyst loading were evaluated under the same circumstances. The polarization curves produced by graphing the current density (J) versus the applied potential (V) in 0.5 M H_2SO_4 are shown in Figure 6d. The current densities of h-BN, MoS_2, h-BN/MoS_2, and Ge/h-BN/MoS_2 are −2.2, −2.9, −4.2, and 13.5 mA/cm^2, respectively. The Ge/h-BN/MoS_2 nanohybrid electrode showed an overall potential at −13.5 mA/cm^2 and low overpotential (η_{10}) of 0.57 mV to reach "J" cathodic 5 mA/cm^2. Similarly, pristine BN and MoS_2 exhibited lower HER electrocatalytic activity, with overall potentials of −2.2 and −2.9 mV, respectively. Over the studied potential range, the blank boron nitride was shown to have minimal HER activity. Similarly, the Tafel plot demonstrates the electrocatalytic process implicated in the HER (overpotential

versus log j). The Tafel slopes of the Ge/h-BN/MoS_2 nanohybrid, nanostructured h-BN/MoS_2, MoS_2, and BN were calculated as 204, 203, 671, and 220 mV dec^{-1}, respectively (Figure 6e).

5. Conclusions

In summary, the Ge/h-BN/MoS_2 heterostructure was successfully synthesized using a simple chemical method. Efficient interface design, defect engineering, phase modification, and activated edges are beneficial for boosting the performance of materials in electrochemical energy conversion and storage. The present work justifies the report on the facile approach to fabricating two-dimensional (2D) Ge-decorated h-BN/MoS_2 heterostructure nanosheets by self-assembly. The physicochemical link between germanium modulation on heterostructure boron nitride/molybdenum sulphide (Ge/h-BN/MoS_2) and oxygen/hydrogen evolution reaction (HER/OER) is better organised when there are more active sites. Moreover, the Ge-decorated h-BN/MoS_2 catalyst realised an overall potential value with RHE of 17.1 (OER) and −13.5 (HER) at 5 mA/cm^2, Tafel value of ∼204 mV/dec (HER), and long-term electrolysis stability of 10 h. The CV curve shows remarkable specific capacitance up to 927.78 F g^{-1} at a scan rate of 10 mV s^{-1}, due to the introduction of Ge onto the h-BN/MoS_2 composite. Even at a lower scan rate, 10 mV s^{-1}, the capacitance delivered is satisfactory, at 546.26 F g^{-1}. The GCD curve shows the addition of Ge to the h-BN/MoS_2 composite amplified the capacitance to 558.53 F g^{-1} at 1 A g^{-1} current density and 159.19 F g^{-1} at 10 A g^{-1}. With a capacitance retention ratio of 85.69% over 2000 cycles, the electrode has outstanding cyclic stability. The results presented in this work show that building the electrode material into a stable structure improves its electrochemical performance significantly. Overall, these results show that a 2D germanium ion on heterostructure, ultrathin h-BN/MoS_2 electrodes is good for electrochemical devices that convert and store energy.

Author Contributions: Conceptualization, M.S. and R.P.; Methodology, M.S., P.S.K. and R.J.K.; Validation, M.S., R.P., P.S.V., N.K., K.A. and J.K.; Formal analysis, V.S., K.D., P.S.V. and N.K.; Investigation, M.S. and R.P.; Resources, K.A.; Data curation, M.S. and R.P.; Writing—original draft, M.S., R.P. and V.S.; Writing—review & editing, V.S., K.D., P.S.K., R.J.K. and K.A.; Visualization, J.K.; Supervision, K.A. and J.K.; Project administration, J.K. All authors have read and agreed to the published version of the manuscript.

Funding: This research was supported by the National Research Foundation of Korea (NRF) grant funded by the Republic of Korea government (MSIT) (No. 2022R1A2C1005357).

Data Availability Statement: Not applicable.

Conflicts of Interest: The authors declare no conflict of interest.

References

1. Thakur, A.K.; Majumder, M.; Choudhary, R.B.; Singh, S.B. MoS_2 flakes integrated with boron and nitrogen-doped carbon: Striking gravimetric and volumetric capacitive performance for supercapacitor applications. *J. Power Sources* **2018**, *402*, 163–173. [CrossRef]
2. Sarmah, D.; Kumar, A. Symmetric supercapacitors with layer-by-layer molybdenum disulfide-reduced graphene oxide structures and poly (3, 4-ethylenedioxythiophene) nanoparticles nanohybrid electrode. *J. Energy Storage* **2021**, *35*, 102289. [CrossRef]
3. Krishnaiah, P.; Kumar, B.P.P.K.Y.; Asha, P.K.; Nautiyal, P.; Devi, V.A.; Alharthi, F.A.; Parashuram, L.; Raghu, M.S. Fabrication of anode material for asymmetric supercapacitor device using polyaniline wrapped boron carbon nitride nanocomposite with enhanced capacitance. *J. Alloy. Compd.* **2020**, *848*, 156602. [CrossRef]
4. Cheng, P.; Yuan, C.; Zhou, Q.; Hu, X.; Li, J.; Lin, X.; Wang, X.; Jin, M.; Shui, L.; Gao, X.; et al. Core–shell MoS_2@ CoO electrocatalyst for water splitting in neural and alkaline solutions. *J. Phys. Chem. C* **2019**, *123*, 5833–5839. [CrossRef]
5. Sun, Y.Y.; Jiang, M.Y.; Wu, L.K.; Hou, G.Y.; Liu, Y.P.T.M. Ultra-thin NiFeSe nanosheets as a highly efficient bifunctional electrocatalyst for overall water splitting. *Sustain. Energy Fuels* **2020**, *4*, 582–588. [CrossRef]
6. Wang, Q.; Zhao, Z.L.; Dong, S.; He, D.; Lawrence, M.J.; Han, S.; Cai, C.; Xiang, S.; Rodriguez, P.; Xiang, B.; et al. Design of active nickel single-atom decorated MoS_2 as a pH-universal catalyst for hydrogen evolution reaction. *Nano Energy* **2018**, *53*, 458–467. [CrossRef]
7. Guan, S.; Fu, X.; Lao, Z.; Jin, C.; Peng, Z. NiS–MoS_2 hetero-nanosheet array electrocatalysts for efficient overall water splitting. *Sustain. Energy Fuels* **2019**, *3*, 2056–2066. [CrossRef]

8. An, T.; Wang, Y.; Tang, J.; Wei, W.; Cui, X.; Alenizi, A.M.; Zhang, L.; Zheng, G. Interlaced NiS_2–MoS_2 nanoflake-nanowires as efficient hydrogen evolution electrocatalysts in basic solutions. *J. Mater. Chem. A* **2016**, *4*, 13439–13443. [CrossRef]
9. He, H.Y.; He, Z.; Shen, Q. Efficient hydrogen evolution catalytic activity of graphene/metallic MoS_2 nanosheet heterostructures synthesized by a one-step hydrothermal process. *Int. J. Hydrogen Energy* **2018**, *43*, 21835–21843. [CrossRef]
10. Vikraman, D.; Hussain, S.; Akbar, K.; Truong, L.; Kathalingam, A.; Chun, S.H.; Jung, J.; Park, H.J.; Kim, H.S. Improved hydrogen evolution reaction performance using MoS_2–WS_2 heterostructures by physicochemical process. *ACS Sustain. Chem. Eng.* **2018**, *6*, 8400–8409. [CrossRef]
11. Padmanaban, A.; Padmanathan, N.; Dhanasekaran, T.; Manigandan, R.; Srinandhini, S.; Sivaprakash, P.; Arumugam, S.; Narayanan, V. Hexagonal phase Pt-doped cobalt telluride magnetic semiconductor nanoflakes for electrochemical sensing of dopamine. *J. Electroanal. Chem.* **2020**, *877*, 114658. [CrossRef]
12. Kou, Z.; Wang, T.; Gu, Q.; Xiong, M.; Zheng, L.; Li, X.; Pan, Z.; Chen, H.; Verpoort, F.; Cheetham, A.K.; et al. Rational design of holey 2D non-layered transition metal carbide/nitride heterostructure nanosheets for highly efficient water oxidation. *Adv. Energy Mater.* **2019**, *9*, 1803768. [CrossRef]
13. Qiu, B.; Cai, L.; Wang, Y.; Lin, Z.; Zuo, Y.; Wang, M.; Chai, Y. Fabrication of nickel–cobalt bimetal phosphide nanocages for enhanced oxygen evolution catalysis. *Adv. Funct. Mater.* **2018**, *28*, 1706008. [CrossRef]
14. Zhao, Y.; Jin, B.; Vasileff, A.; Jiao, Y.; Qiao, S.Z. Interfacial nickel nitride/sulfide as a bifunctional electrode for highly efficient overall water/seawater electrolysis. *J. Mater. Chem. A* **2019**, *7*, 8117–8121. [CrossRef]
15. Chang, K.; Hai, X.; Pang, H.; Zhang, H.; Shi, L.; Liu, G.; Liu, H.; Zhao, G.; Li, M.; Ye, J. Targeted synthesis of 2H-and 1T-phase MoS_2 monolayers for catalytic hydrogen evolution. *Adv. Mater.* **2016**, *28*, 10033–10041. [CrossRef] [PubMed]
16. Herrera-Reinoza, N.; Santos, A.C.D.; de Lima, L.H.; Landers, R.; de Siervo, A. Atomically precise bottom-up synthesis of h-BNC: Graphene doped with h-BN nanoclusters. *Chem. Mater.* **2021**, *33*, 2871–2882. [CrossRef]
17. Wu, Y.; Huang, Z.; Liu, H.; He, C.; Xue, L.; Qi, X.; Zhong, J. Transition metal atoms absorbed on MoS_2/h-BN heterostructure: Stable geometries, band structures and magnetic properties. *Phys. Chem. Chem. Phys.* **2018**, *20*, 17387–17392. [CrossRef]
18. Tronganh, N.; Yang, Y.; Chen, F.; Lu, M.; Jiang, Y.; Gao, Y.; Cheng, L.; Jiao, Z. SiO_2-assisted synthesis of layered MoS_2/reduced graphene oxide intercalation composites as high performance anode materials for Li-ion batteries. *RSC Adv.* **2016**, *6*, 74436–74444. [CrossRef]
19. Iyyamperumal, E.; Wang, S.; Dai, L. Vertically aligned BCN nanotubes with high capacitance. *ACS Nano* **2012**, *6*, 5259–5265. [CrossRef]
20. Liu, J.; Chen, X.; Kim, J.; Zheng, Q.; Ning, H.; Sun, P.; Huang, X.; Liu, J.; Niu, J.; Braun, P.V. High volumetric capacity three-dimensionally sphere-caged secondary battery anodes. *Nano Lett.* **2016**, *16*, 4501–4507. [CrossRef]
21. Chen, L.; Yang, Y.; Gao, Y.; Tronganh, N.; Chen, F.; Lu, M.; Jiang, Y.; Jiao, Z.; Zhao, B. Facile synthesis of ultrathin, undersized MoS_2/graphene for lithium-ion battery anodes. *RSC Adv.* **2016**, *6*, 99833–99841. [CrossRef]
22. Zhao, B.; Wang, Z.; Gao, Y.; Chen, L.; Lu, M.; Jiao, Z.; Jiang, Y.; Ding, Y.; Cheng, L. Hydrothermal synthesis of layer-controlled MoS_2/graphene composite aerogels for lithium-ion battery anode materials. *Appl. Surf. Sci.* **2016**, *390*, 209–215. [CrossRef]
23. Palanisamy, R.; Karuppiah, D.; Venkatesan, S.; Mani, S.; Kuppusamy, M.; Marimuthu, S.; Karuppanan, A.; Govindaraju, R.; Marimuthu, S.; Rengapillai, S.; et al. High-performance asymmetric supercapacitor fabricated with a novel MoS_2/Fe_2O_3/Graphene composite electrode. *Colloids Interface Sci. Commun.* **2022**, *46*, 100573. [CrossRef]
24. Seki, T.; Chiang, K.-Y.; Yu, C.-C.; Yu, X.; Okuno, M.; Hunger, J.; Nagata, Y.; Bonn, M. The Bending Mode of Water: A Powerful Probe for Hydrogen Bond Structure of Aqueous Systems. *J. Phys. Chem. Lett.* **2020**, *11*, 8459–8469. [CrossRef] [PubMed]
25. Pálinkó, I.; Sipos, P.; Berkesi, O.; Varga, G. Distinguishing Anionic Species That Are Intercalated in Layered Double Hydroxides from Those Bound to Their Surface: A Comparative IR Study. *J. Phys. Chem. C* **2022**, *126*, 15254–15262. [CrossRef]
26. Liu, J.; Zhang, L.; Li, N.; Tian, Q.; Zhou, J.; Sun, Y. Synthesis of MoS_2/$SrTiO_3$ composite materials for enhanced photocatalytic activity under UV irradiation. *J. Mater. Chem. A* **2015**, *3*, 706–712. [CrossRef]
27. Giribabu, K.; Oh, S.Y.; Suresh, R.; Kumar, S.P.; Manigandan, R.; Munusamy, S.; Gnanamoorthy, G.; Kim, J.Y.; Huh, Y.S.; Narayanan, V. Sensing of picric acid with a glassy carbon electrode modified with CuS nanoparticles deposited on nitrogen-doped reduced graphene oxide. *Microchim. Acta.* **2016**, *183*, 2421–2430. [CrossRef]
28. Pandit, M.A.; Kumar, D.S.H.; Billakanti, S.; Ramadoss, M.; Muralidharan, K. Chalcopyrite with Magnetic and Dielectric Properties: An Introductory Catalyst for 4-Nitrophenol Reduction. *J. Phys. Chem. C* **2020**, *124*, 18010–18019. [CrossRef]
29. Zhao, Z.; Xie, Y. Electrochemical supercapacitor performance of boron and nitrogen co-doped porous carbon nanowires. *J. Power Sources* **2018**, *400*, 264–276. [CrossRef]
30. Abraham, A.M.; Lonkar, S.P.; Pillai, V.V.; Alhassan, S.M. Three-Dimensional MoS_2 Nanodot-Impregnated Nickel Foam Electrodes for High-Performance Supercapacitor Applications. *ACS Omega* **2020**, *5*, 11721–11729. [CrossRef]
31. Li, X.; Zhang, C.; Xin, S.; Yang, Z.; Li, Y.; Zhang, D.; Yao, P. Facile synthesis of MoS_2/reduced grapheneoxide@polyaniline for high-performance supercapacitors. *ACS Appl. Mater. Interfaces* **2016**, *8*, 21373–21380. [CrossRef] [PubMed]
32. Manuraj, M.; Nair, K.K.; Unni, K.N.; Rakhi, R.B. High performance supercapacitors based on MoS_2 nanostructures with near commercial mass loading. *J. Alloys Compd.* **2020**, *819*, 152963. [CrossRef]
33. Li, R.; Qin, C.; Zhang, X.; Lin, Z.; Jiang, S.L.X. Boron/nitrogen co-doped carbon synthesized from waterborne polyurethane and graphene oxide composite for supercapacitors. *RSC Adv.* **2019**, *9*, 1679–1689. [CrossRef] [PubMed]

34. Xie, K.; Zhang, M.; Yang, Y.; Zhao, L.; Qi, W. Synthesis and supercapacitor performance of polyaniline/nitrogen-doped ordered mesoporous carbon composites. *Nanoscale Res. Lett.* **2018**, *13*, 1–8. [CrossRef]
35. Liu, J.; Du, P.; Wang, Q.; Liu, D.; Liu, P. Mild synthesis of holey N-doped reduced graphene oxide and its double-edged effects in polyaniline hybrids for supercapacitor application. *Electrochim. Acta* **2019**, *305*, 175–186. [CrossRef]
36. Guevara, D.; Boscá, A.; Pedrós, A.J.; Climent, P.E.; Andrés, D.A.; Calle, F. Reduced graphene oxide/polyaniline electrochemical supercapacitors fabricated by laser. *Appl. Surf. Sci.* **2019**, *467–468*, 691–697. [CrossRef]
37. Hao, Q.; Xia, X.; Lei, W.; Wang, W.; Qiu, J. Facile synthesis of sandwich-like polyaniline/boron-doped graphenenano hybrid for supercapacitors. *Carbon* **2015**, *81*, 552–563. [CrossRef]
38. Dhanasekaran, T.; Manigandan, R.; Padmanaban, A.; Suresh, R.; Giribabu, K.; Narayanan, V. Fabrication of Ag@Co-Al Layered Double Hydroxides Reinforced poly(o-phenylenediamine) Nanohybrid for Efficient Electrochemical Detection of 4-Nitrophenol, 2,4-Dinitrophenol and Uric acid at Nano Molar Level. *Sci. Rep.* **2019**, *9*, 13250. [CrossRef]